Dalton Transactions

ROYAL SOCIETY OF CHEMISTRY

PAPER

View Article Online
View Journal | View Issue

Cite this: *Dalton Trans.*, 2026, **55**, 5553

Fraternal twins: B_2O_2- or B_2N_2-doped polycyclic π systems and their formation mechanism *via* regiodivergent Au- *versus* amine-catalyzed cyclizations

Simon M. Mittag, [a] Jonas Klopf,[b] Alexander V. Virovets, [a] Eugenia Peresypkina, [a] Hans-Wolfram Lerner, [a] Holger Helten *[b] and Matthias Wagner *[a]

Received 16th February 2026,
Accepted 26th February 2026

DOI: 10.1039/d6dt00412a

rsc.li/dalton

BE-doped polycyclic aromatic hydrocarbons (PAHs; E = NR, O) often exhibit superior optoelectronic properties compared to their carbonaceous congeners. Herein, we report an efficient and convenient synthetic route to this compound class, based on the intramolecular addition of aryl(Mes)BE–H bonds to *ortho*-positioned butadiyne substituents. The reactions can proceed either under Au(I) or NEt_3 catalysis, with the same substrate giving rise to distinct addition patterns. Treatment of *o*-MesB(OH)-diphenylbutadiyne or *o*,*o*′-bis[MesB(OH)]-diphenylbutadiyne with $[Au(PPh_3)(NTf_2)]$ furnishes an ethynyl-substituted BO-naphthalene or a $(BO)_2$-binaphthyl (**B_2O_2**; *via* 2,3-OC-addition), respectively. In contrast, NEt_3-catalyzed double cyclization of *o*,*o*′-bis[MesB(OH)]-diphenylbutadiyne affords the corresponding $(BO)_2$-naphthylbenzofulvene (*iso*-**B_2O_2**; *via* 1,3-OC-addition). Replacement of NEt_3 with ethylenediamine generates the analogous $(BN)_2$-doped PAH (*iso*-**B_2N_2**). Notably, both **B_2O_2** and *iso*-**B_2N_2** show high photoluminescence quantum yields of Φ_{PL} = 80% and 93%, respectively. Using the formation of *iso*-**B_2O_2** as a model reaction, a plausible mechanistic scenario was elucidated through quantum-chemical calculations and systematic probe experiments, providing further novel BE-doped PAHs.

Introduction

Incorporating p-block elements into polycyclic aromatic hydrocarbons (PAHs) is a powerful strategy for generating new molecules with diverse applications in drug development, catalysis, and materials science.[1–3] A particularly successful approach is to replace selected nonpolar $R_2C{=}CR_2$ bonds with isosteric, polar $R_2B{=}ER$ units (E = NR, O), thereby reshaping electronic properties by modulating π-electron distributions and frontier-orbital energies.[4–8] Systematically varying the position, orientation, and number of incorporated $R_2B{=}ER$ groups further expands the range of accessible architectures with physical properties that can differ substantially from those of their carbon analogues.[9–12] Moreover, the symmetry breaking associated with $R_2B{=}ER$ incorporation frequently enhances regioselectivity in late-stage functionalization and alters intermolecular interactions in supramolecular assemblies and the solid state.[13,14]

We have recently disclosed an atom-economical synthetic approach to singly or multiply $(BE)_n$-doped PAHs from readily available, easy-to-handle *ortho*-alkynyl-substituted phenylborinic acids **I** (Fig. 1a).[15,16] In the key step, the Au(I) complex $[Au(PPh_3)NTf_2]$ catalyzes the intramolecular 6-*endo-dig* addition of the BO–H bonds across the C≡C units, generating six-membered (BO)-heterocycles (Tf: SO_2CF_3). Remarkable modularity is achieved by converting the borinic acids into aminoborane intermediates *via* reaction with silylated amines. These aminoboranes likewise undergo Au(I)-catalyzed cyclization, thereby providing access to (BN)-heterocycles (Fig. 1a).[15,16]

To further expand the accessible chemical space, we now turned from *ortho*-alkynyl- to *ortho*-butadiynyl-substituted starting materials. This modification promises several benefits: (i) monocyclization at a butadiyne unit should directly afford ethynyl-substituted $(BE)_n$-heterocycles (Fig. 1a; R: C≡CR′), typically associated with bathochromic emission shifts and enhanced photoluminescence quantum yields (Φ_{PL}; *cf.* compounds **III** *vs.* **IV** in Fig. 1b).[17–19] (ii) A butadiyne bridge between two phenylborinic acid moieties should enable double cyclization, potentially providing two directly connected (BO)- or (BN)-PAHs in a single step (*cf.* **V** and **VI** in Fig. 1c). Comparison with their carbonaceous congener binaphthyl **VII** furthermore allows

[a]*Goethe-Universität Frankfurt, Institut für Anorganische und Analytische Chemie, Max-von-Laue-Straße 7, D-60438 Frankfurt (Main), Germany. E-mail: matthias.wagner@chemie.uni-frankfurt.de*
[b]*Julius-Maximilians-Universität Würzburg, Institute of Inorganic Chemistry and Institute for Sustainable Chemistry & Catalysis with Boron (ICB), Am Hubland, D-97074 Würzburg, Germany. E-mail: holger.helten@uni-wuerzburg.de*

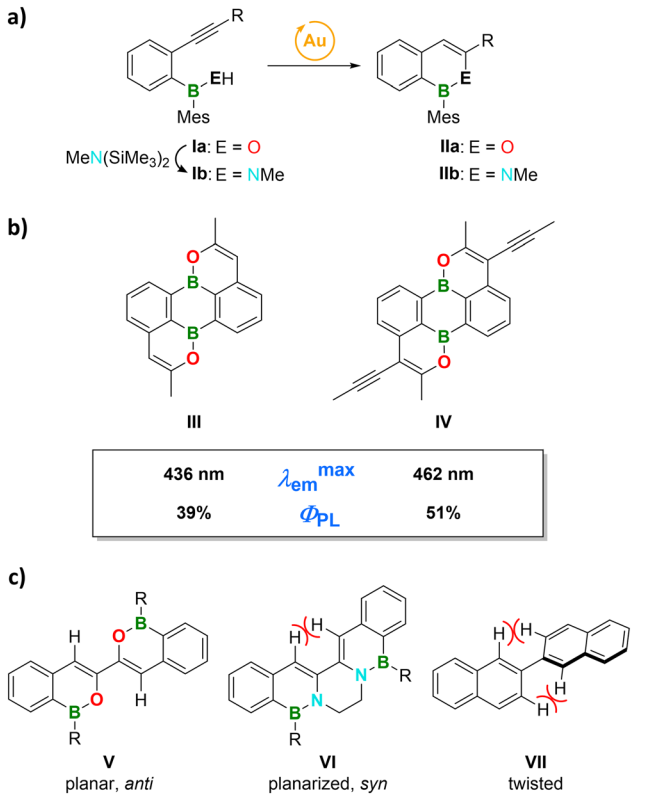

Fig. 1 (a) Au(I)-catalyzed cyclization of *ortho*-alkynyl-substituted phenylborinic acids (**Ia**) and aminoboranes (**Ib**) to afford (BE)-naphthalenes (**IIa**, **b**; E = NMe, O; R = alkyl, aryl).[15,16] (b) Representative examples of $(BO)_2$-doped PAHs without (**III**) and with alkynyl substituents (**IV**), highlighting the beneficial impact of the latter on key photoluminescence properties.[15,19] (c) Effect of $(BE)_2$-doping on the conformational characteristics of 2,2′-binaphthyl derivatives (**V**–**VII**).

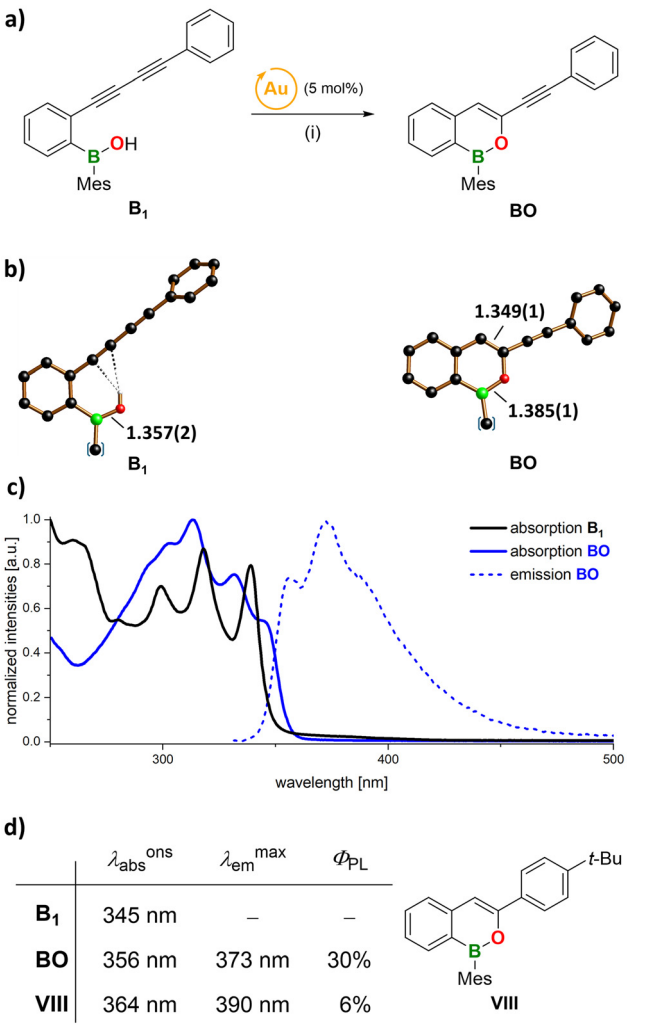

Fig. 2 (a) Synthesis of phenylethynyl-substituted BO-naphthalene **BO** from the butadiynyl-substituted borinic acid $\mathbf{B_1}$. Reagents and conditions: (i) 0.05 eq. $[Au(PPh_3)(NTf_2)]$, MTBE, rt, 12 h, 82%. (b) Molecular structures of $\mathbf{B_1}$ (left) and **BO** (right) in the solid state. H: white, B: green, C: black, O: red. For clarity, only the *ipso*-C atoms of the Mes substituents are shown; C–*H* atoms are omitted. The bond lengths are given in [Å]. (c) Normalized UV/Vis absorption (solid lines) and emission (dashed line) spectra of $\mathbf{B_1}$ and **BO** in C_6H_{12} (compound $\mathbf{B_1}$ does not show detectable photoluminescence). (d) Absorption and photoluminescence properties of $\mathbf{B_1}$, **BO**, and **VIII**[16] in C_6H_{12} (λ_{abs}^{ons}: absorption onset; λ_{em}^{max}: emission-band maximum; Φ_{PL}: photoluminescence quantum yield).[31]

one to investigate how (BE)-doping influences the conformational preferences of biaryls (*e.g.*, twisted *vs.* planar, *syn vs. anti*; Fig. 1c) and to study the resulting effects on their optoelectronic properties.[20–23] (iii) The binaphthyl scaffold **VII** represents a prominent lead structure for important classes of pharmaceuticals, such as gossypol-type drugs.[24,25] Given the emerging role of boron as a 'magic element' in biomedical science,[26] facile access to $(BN)_2$- and $(BO)_2$-doped gossypol analogs could prove particularly valuable.[27,28]

Experimentally, the Au(I)-catalyzed cyclization of the *ortho*-butadiynyl-substituted phenylborinic acid $\mathbf{B_1}$ proceeds as envisioned, affording the BO-naphthalene **BO** with enhanced optoelectronic properties (Fig. 2a). The butadiyne-bridged precursor $\mathbf{B_2}$ likewise undergoes the anticipated twofold cycloaddition to give the $(BO)_2$-binaphthyl $\mathbf{B_2O_2}$ (**V**-type compound with R = Mes) in high yields. However, the corresponding reaction in the presence of ethylenediamine diverges markedly from the *a priori* expected selectivity, as it generates the naphthylbenzofulvene isomer *iso*-$\mathbf{B_2N_2}$ instead of binaphthyl **VI** (Fig. 1 and 3). Even more intriguingly, this transformation proceeds spontaneously and is not influenced by the presence or absence of the Au(I) complex. An important lesson learned from this serendipitous finding is that $\mathbf{B_2}$ can also undergo an amine-catalyzed cyclization, which, however, furnishes not $\mathbf{B_2O_2}$ but its isomer *iso*-$\mathbf{B_2O_2}$ (Fig. 3). A major part of this work is therefore devoted to elucidating these contrasting pathways both experimentally and computationally.

Results and discussion

The synthesis and full characterization of the *ortho*-butadiynyl-substituted arylborinic acid starting materials $\mathbf{B_1}$ (Fig. 2) and $\mathbf{B_2}$ (Fig. 3) are provided in the SI.

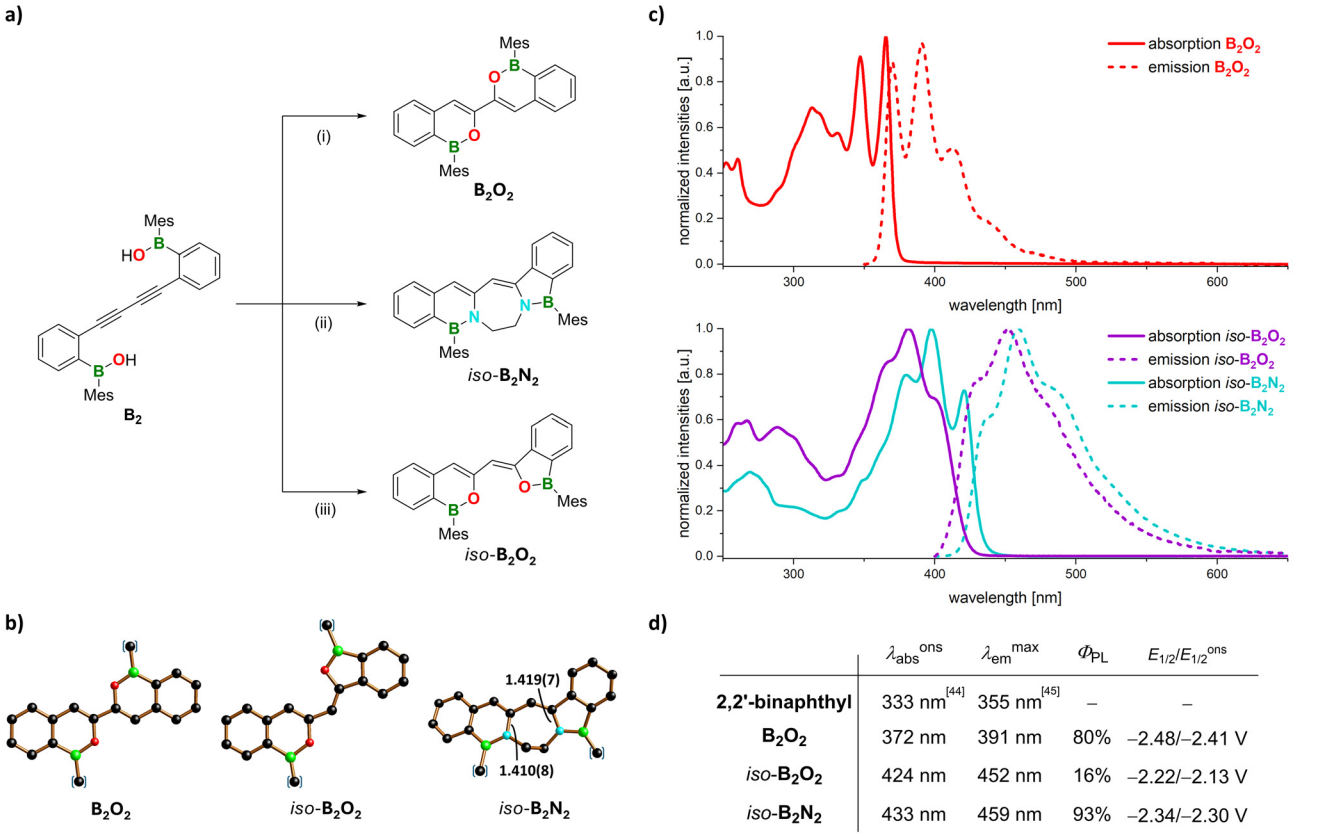

	λ_{abs}^{ons}	λ_{em}^{max}	Φ_{PL}	$E_{1/2}/E_{1/2}^{ons}$
2,2'-binaphthyl	333 nm[44]	355 nm[45]	–	–
B_2O_2	372 nm	391 nm	80%	–2.48/–2.41 V
***iso*-B_2O_2**	424 nm	452 nm	16%	–2.22/–2.13 V
***iso*-B_2N_2**	433 nm	459 nm	93%	–2.34/–2.30 V

Fig. 3 (a) Synthesis of the $(BO)_2$-binaphthyl B_2O_2 and the $(BE)_2$-naphthylbenzofulvenes *iso*-B_2N_2 and *iso*-B_2O_2. Reagents and conditions: (i) 0.05 eq. $[Au(PPh_3)(NTf_2)]$, MTBE, rt, 12 h, 93%. (ii) 1 eq. ethylenediamine, THF, rt, 12 h, 82%. (iii) 2 eq. *i*-Pr_2NH, THF, 60 °C, 12 h, 61% (conversion according to ^1H NMR spectroscopy ≈ 90%). (b) Molecular structures of B_2O_2 (left), *iso*-B_2O_2 (middle), *iso*-B_2N_2 (right) in the solid state. B: green, C: black, N: cyan, O: red. For clarity, only the *ipso*-C atoms of the Mes substituents are shown; H atoms are omitted. (c) Normalized UV/Vis absorption (solid lines) and emission (dashed lines) spectra of B_2O_2 (top) and *iso*-B_2O_2/*iso*-B_2N_2 (bottom) in C_6H_{12}. (d) Photophysical and electrochemical data of the compounds 2,2'-binaphthyl, B_2O_2, *iso*-B_2O_2, and *iso*-B_2N_2. Electronic spectra of B_2O_2, *iso*-B_2O_2, and *iso*-B_2N_2 were recorded in C_6H_{12} (see the SI for the measurements in C_6H_6, $CHCl_3$, THF solutions, or in a PMMA layer); the corresponding values for 2,2'-binaphthyl were reported in *n*-pentane (λ_{abs}^{ons})[44] and Me-C_6H_{11} (λ_{em}^{max});[45] cyclic voltammograms were recorded in THF and referenced to the FcH/FcH^+ couple (supporting electrolyte: 0.1 M $[n\text{-}Bu_4N][PF_6]$, scan rate: 200 mV s^{-1}).[31]

Synthesis and characterization of the alkynyl-substituted BO-naphthalene BO

Treatment of the monoborinic acid $\mathbf{B_1}$ with 5 mol% of the cyclization catalyst $[Au(PPh_3)(NTf_2)]$ in methyl *tert*-butyl ether (MTBE) affords the phenylethynyl-substituted BO-naphthalene **BO** in 82% yield (Fig. 2a; see the SI for the analogous compound $\mathbf{BO}^{SI}$, bearing a *t*-Bu substituent in place of the Ph ring). In the ^1H and $^{13}C\{^1H\}$ NMR spectra ($CDCl_3$), successful cyclization to **BO** is indicated by two features: (i) the O–*H* resonance of $\mathbf{B_1}$ (7.74–7.60 ppm; br) vanishes, while a new singlet at 7.08 ppm appears, attributable to the vinyl proton of **BO**; (ii) the number of resonances assignable to $^{13}C(sp)$ atoms decreases from four in $\mathbf{B_1}$ to two in **BO**. The solid-state structures of $\mathbf{B_1}$ and **BO** reveal B–O bond lengths of 1.357(2) and 1.385(1) Å, respectively (Fig. 2b). This elongation (Δ(B–O) = 0.028 Å) upon cyclization is consistent with partial delocalization of the π-electron density originally localized between B and O in the ring-opened system. The C=C bond length of the newly formed vinyl moiety [1.349(1) Å] is essentially identical to that of the C(9)=C(10) bond in phenanthrene [1.351 Å],[29] which possesses a highly olefinic nature.[30] Borinic acid $\mathbf{B_1}$ is a colorless, non-fluorescent solid. Upon cyclization to **BO**, the onset of the UV/Vis absorption band remains largely unaffected, but fluorescence emerges at λ_{em}^{max} = 373 nm (C_6H_{12}).[31] The intended alkynyl substituent-induced emission enhancement is achieved, with Φ_{PL} increasing from 6% to 30% when comparing the phenyl-substituted BO-naphthalene **VIII** with its phenylethynyl-substituted congener **BO** (Fig. 2c and d).[16]

Synthesis and characterization of the $(BO)_2$-binaphthyl B_2O_2 and the $(BE)_2$-naphthylbenzofulvenes *iso*-B_2O_2 and *iso*-B_2N_2

The butadiynylene-bridged bisborinic acid $\mathbf{B_2}$ undergoes double cyclization in the presence of the Au(I) catalyst to furnish the $(BO)_2$-binaphthyl $\mathbf{B_2O_2}$ (93% yield; Fig. 3a). An analogous π-extended $(BO)_2$-bianthryl was obtained using the same approach ($\mathbf{B_2O_2}^{SI}$; see the SI for details). In contrast, treating $\mathbf{B_2}$ with 1 eq. of ethylenediamine triggers a one-pot

reaction cascade that forms two B–N and two C–N bonds, even in the absence of [Au(PPh$_3$)(NTf$_2$)] (Fig. 3a). The product *iso*-**B$_2$N$_2$** (82% yield) contains one six- and one five-membered B-containing heterocycle, rather than the two six-membered heterocycles found in **B$_2$O$_2$** and originally anticipated for **VI** (Fig. 1c). The ethylene bridge linking the two N atoms additionally generates a central seven-membered ring (see the SI for the analogous compound *iso*-**B$_2$N$_2$**^{SI}, containing an eight-membered ring and a propylene chain between the two N atoms). Notably, the reaction outcome does not depend on the presence of the Au(I) catalyst or the timing of its addition, as comparable yields of *iso*-**B$_2$N$_2$** were obtained in all cases. We therefore propose that, beyond serving as a stoichiometric reagent, ethylenediamine mediates its own hydroamination reaction,[32] favoring six-/five- over six-/six-membered ring formation and overriding the intrinsic six/six-selectivity of the Au(I) catalyst (when present).

To test this assumption, we heated a mixture of **B$_2$** and *i*-Pr$_2$NH in THF at 60 °C for 12 h. After chromatographic workup, the double-cyclization product *iso*-**B$_2$O$_2$** was isolated in 61% yield (90% conversion by ^{1}H NMR). In stark contrast to **B$_2$O$_2$**, *iso*-**B$_2$O$_2$** features the same six-/five-membered heterocyclic motif as *iso*-**B$_2$N$_2$**, again suggesting that the connectivity is governed primarily by the catalyst (Au(I) *vs.* amine), whereas the nucleophilic moiety (NH *vs.* OH) is less influential.

A high average symmetry of **B$_2$O$_2$** in solution is evidenced by a single set of ^{1}H- and ^{13}C NMR signals, corresponding to one half of the molecule. In *iso*-**B$_2$O$_2$**, however, all H and C atoms are magnetically unique. The endocyclic vinylic CH units of **B$_2$O$_2$** resonate at $\delta(^1\text{H})$ = 7.61 and $\delta(^{13}\text{C})$ = 108.6. In contrast, *iso*-**B$_2$O$_2$** features one endocyclic and one exocyclic vinylic CH moiety, giving rise to signals at 7.92/113.6 ppm and 6.56/103.9 ppm, respectively. Thus, the C atoms in β positions to the π-donating O atoms are significantly shielded, reflecting considerable accumulation of negative charge,[33–36] which is slightly more pronounced for the exocyclic CH fragment in *iso*-**B$_2$O$_2$**. The main differences between the ^{13}C{^{1}H} NMR spectra of *iso*-**B$_2$N$_2$** and *iso*-**B$_2$O$_2$** are (i) a lower degree of deshielding of the N-appended vinylic C atoms compared to those attached to the more electronegative O atoms (140.9/144.4 ppm *vs.* 149.3/155.7 ppm), and (ii) the presence of two signals at 48.9/51.9 ppm, assignable to the ethylene bridge. Moreover, four Mes-*o*-CH$_3$ resonances in the spectrum of *iso*-**B$_2$N$_2$** *vs.* two in that of *iso*-**B$_2$O$_2$** suggest sterically hindered rotation of both NB–Mes substituents, while the OB–Mes groups remain freely rotating.

The proposed molecular structures of **B$_2$O$_2$**, *iso*-**B$_2$O$_2$**, and *iso*-**B$_2$N$_2$** were confirmed by single-crystal X-ray diffraction (SCXRD; Fig. 3b). The (BO)$_2$-binaphthyl core of **B$_2$O$_2$** is centrosymmetric and perfectly planar. Its O atoms adopt an *anti*-arrangement across the central C–C bond, thereby avoiding the electronic and steric repulsions that would arise in *syn*-**B$_2$O$_2$** between the O-atom lone pairs on the one hand and the C–H vectors oriented toward the bay region on the other.

The **B$_2$O$_2$** isomer *iso*-**B$_2$O$_2$** is also planar in the solid state. NMR spectroscopy had suggested a structure comprising a BO-naphthyl unit linked *via* its exocyclic C atom to a BO-benzofulvene fragment, which is now confirmed. With respect to the central formal C–C single bond, *iso*-**B$_2$O$_2$** possesses an *anti*-conformation, such that the two O atoms are again maximally separated. Each C_1-symmetric molecule of *iso*-**B$_2$O$_2$** is positionally disordered about a crystallographically imposed inversion center.

Similar to *iso*-**B$_2$O$_2$**, compound *iso*-**B$_2$N$_2$** suffers from whole-molecule disorder in the crystal lattice: two differently oriented molecules, related by a pseudo-twofold axis, overlap in the same position (see the SI for more details). Nevertheless, the sequence of six/seven/five-membered rings within the molecule's heterocyclic core is unequivocally discernible. The dihedral angle between the two planar, benzannulated heterocycles is only av. 19.0[1]°;[37] the ethylene bridge is twisted out of the best-fit plane through the main molecular framework. The two N–C(sp^2) bonds measure 1.410(8) Å and 1.419(7) Å, which markedly exceed the N–C bond lengths in, *e.g.*, the methylpyridinium salt [MeNC$_5$H$_5$][BPh$_4$] (av. 1.337[4] Å;[37] CSD: ACINOP),[38] and thus exhibit considerable single-bond character. The key geometrical parameters of the formal C–C═C fragment connecting the two BN-heterocycles are comparable to those of the corresponding fragment in *iso*-**B$_2$O$_2$**.

A primary motivation for synthesizing **B$_2$O$_2$** was the expectation that BO-doping would impart optoelectronic properties superior to those of the hydrocarbon 2,2′-binaphthyl, owing to facilitated planarization and the concomitant extension of π-conjugation.[20] According to quantum-chemical calculations (ωB97X-D/6-311+G(d,p), CPCM(THF)),[39,40] planar *anti*-**B$_2$O$_2$** indeed represents the global minimum not only in the solid state but also in solution, while twisted *syn*-**B$_2$O$_2$** constitutes a local minimum at higher energy (O–C–C–O = 27°; ΔG(*syn–anti*) = 4.3 kcal mol^{-1}). The carbonaceous 2,2′-binaphthyl is likewise *anti*-planar in the crystal lattice (CSD: JAKROC01),[41] but its ground-state torsional potential in solution shows two nearly isoenergetic minima at dihedral angles of approximately ±40°. The higher computed rotational barrier of **B$_2$O$_2$** (9.1 kcal mol^{-1}) compared to 2,2′-binaphthyl (<2.5 kcal mol^{-1})[20,42,43] likely reflects a higher degree of π-delocalization in the planar minimum of the former. In the excited state, π–π interactions become more important, accounting for the tendency of biaryls to adopt a more planar conformation upon electronic excitation.[44] This tendency is observed also for **B$_2$O$_2$**: in the S_1 state the *syn*/*anti*-energy difference decreases to 1.3 kcal mol^{-1}, whereas the rotational barrier triples to 27.2 kcal mol^{-1}.

In line with theory, the onset of the lowest-energy UV/Vis absorption band (λ_{abs}^{ons}) and the emission maximum (λ_{em}^{max}) of **B$_2$O$_2$** are bathochromically shifted by ≈ 39 nm (≈ 3150 cm^{-1})[44] and ≈ 36 nm (≈ 2590 cm^{-1}),[45] respectively, relative to the corresponding values of 2,2′-binaphthyl (Fig. 3d).[46] The fluorescence of **B$_2$O$_2$** extends into the visible region, rendering it a blue emitter. Notably, its quantum yield (Φ_{PL}) reaches 80%, about tenfold higher than that of its "monomer" **VIII** (Fig. 2d).[16,47] The $S_0 \rightarrow S_1$ transitions of **B$_2$O$_2$**, *iso*-**B$_2$O$_2$**, and *iso*-**B$_2$N$_2$** are dominated by HOMO → LUMO excitation (> 90% contribution; $f_{osc} > 1$), with the frontier orbitals

delocalized over the entire binaphthyl/naphthylbenzofulvene cores. The calculations consistently overestimate the transition energies; however, the obtained relative energy values are in qualitative agreement with the experimental data (computed λ_{abs}^{c}: 333 ($\mathbf{B_2O_2}^{c}$) < 373 (*iso*-$\mathbf{B_2O_2}^{c}$) ≈ 374 nm (*iso*-$\mathbf{B_2N_2}^{c}$); see the SI for details).

Absorption and emission of the mixed BO-naphthalene/BO-benzofulvene *iso*-$\mathbf{B_2O_2}$ occur at significantly lower energies than those of $\mathbf{B_2O_2}$, with $\Delta(\lambda_{abs}^{ons})$ = 52 nm (3300 cm^{-1}) and $\Delta(\lambda_{em}^{max})$ = 61 nm (3450 cm^{-1}; Fig. 3c). Exchange of O by N in *iso*-$\mathbf{B_2O_2}$ induces only minor spectral changes (*iso*-$\mathbf{B_2N_2}$ *vs. iso*-$\mathbf{B_2O_2}$: $\Delta(\lambda_{abs}^{ons})$ = 9 nm (490 cm^{-1}) and $\Delta(\lambda_{em}^{max})$ = 7 nm (340 cm^{-1}; Fig. 3d)). The quantum efficiency Φ_{PL} drops markedly from 80% to 16%, but recovers to 93% along the series ($\mathbf{B_2O_2}$ → *iso*-$\mathbf{B_2O_2}$ → *iso*-$\mathbf{B_2N_2}$). The diminished Φ_{PL} of *iso*-$\mathbf{B_2O_2}$ compared to that of $\mathbf{B_2O_2}$ is primarily due to its increased rotational degrees of freedom.

Mechanistic insights into amine-promoted cyclization reactions on the butadiyne $\mathbf{B_2}$

As outlined in the synthesis section, the Au(I)-catalyzed twofold ring-closing reaction on $\mathbf{B_2}$ furnishes exclusively (within experimental detection limits) the $(BO)_2$-binaphthyl $\mathbf{B_2O_2}$. Conversely, *i*-Pr_2NH-mediated addition of the two O–H bonds across the C≡C triple bonds affords the isomeric $(BO)_2$-doped naphthylbenzofulvene *iso*-$\mathbf{B_2O_2}$ in excellent yields. The same connectivity pattern as in *iso*-$\mathbf{B_2O_2}$ is likewise observed in *iso*-$\mathbf{B_2N_2}$, where ethylenediamine either reacts spontaneously or functions as both reactant and promoter. The role of the Au(I) catalyst in alkyne hydroalkoxylations is well established: the soft Lewis acid interacts with the substrate's unsaturated bond in a side-on fashion, reducing its π-electron density and thereby activating it toward nucleophilic attack by the O atom.[48–50] Beyond Au(I), a range of other transition metal ions catalyze hydroalkoxylation and hydroamination reactions;[51–55] in some instances these transformations can also proceed under strongly basic conditions without involvement of a d-block-metal complex (*e.g.*, KOR, $LiNR_2$, Schwesinger superbases).[56–58] The role of the weakly basic amine in our reactions is less clear, as literature precedents (*LP*) are scarce and – to the best of our knowledge – exclusively related to butadiyne substrates:

LP1: Butadiyne and monoamines. Schroth *et al.* reported[59,60] that the conversion of parent butadiyne ($HC^1{\equiv}C^2{-}C^3{\equiv}C^4H$) with secondary amines (HNR_2) is facile but terminates after monoaddition at the 1,2-positions (*cf.* **IX**; Fig. 4). By contrast, the analogous reaction with primary amines (H_2NR) proceeds with a second nucleophilic addition at the 3,4-positions (*cf.* **X** and its tautomers; Fig. 4). Neither 1,4- nor 2,3-, but only 1,3-disubstituted butadienes were observed. The olefinic products were obtained in good yields and predominantly adopt the *Z*-configuration, consistent with nucleophilic *trans*-hydroamination. Importantly, treatment of **IX** with excess H_2NR leads to **X**-type derivatives bearing exclusively N(H)R substituents, indicating partial reversibility of the initial hydroamination by HNR_2. Importantly for the subsequent discussion, addition of alcohols (HOR) to **IX** furnishes 1-amino-3-alkoxybuta-1,3-dienes **XI** (Fig. 4).[61]

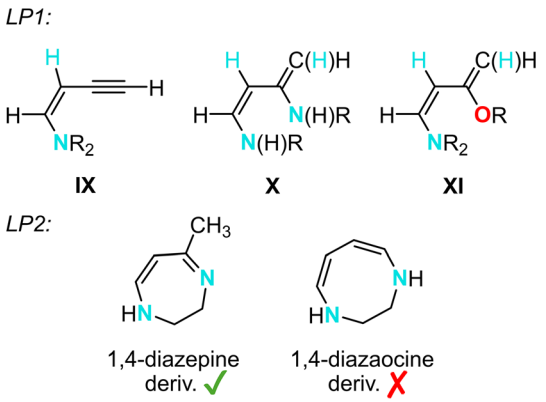

Fig. 4 *LP1*: N–H- and O–H-addition products **IX**–**XI** derived from butadiyne (C_4H_2). Typical reaction conditions: **IX**: neat HNR_2, 30–40 °C; **X**: neat H_2NR, rt; **XI**: (1) neat HNR_2, 30–40 °C, (2) HOR. *LP2*: the seven-membered, partially saturated 1,4-diazepine derivative obtained from ethylenediamine/C_4H_2, and the isomeric eight-membered 1,3-diazaocine, which is not formed.

LP2: Butadiyne and ethylenediamine. Schroth *et al.* and Paudler *et al.* disclosed that the exothermic reaction of butadiyne with excess ethylenediamine affords the seven-membered, partially saturated 1,4-diazepine derivative in near-quantitative yield, rather than the corresponding eight-membered 1,4-diazaocine derivative. This outcome mirrors the 1,3-regioselectivity discussed above for reactions with monoamines.[62–64]

The literature background leaves some open questions that are key for developing a deeper mechanistic understanding of the amine-promoted butadiyne-cyclization reactions investigated here. To fill this gap, we conducted a systematic series of probe experiments (*PE1*–*PE4*) under the conditions employed for synthesizing *iso*-$\mathbf{B_2O_2}$ and *iso*-$\mathbf{B_2N_2}$ (Fig. 5):

PE1 probed whether an active amine catalyst must provide a positively polarized NH-hydrogen atom in lieu of an Au(I) cation to promote BO-heterocycle formation. It turned out that this was not the case, as the tertiary amine NEt_3 proved as effective as the secondary amine *i*-Pr_2NH in generating *iso*-$\mathbf{B_2O_2}$.

PE2 elucidated whether this type of amine catalysis extends to related alkynyl species or is restricted to butadiyne substrates. The latter is true, as the $\mathbf{B_2}$ analogue **XII**, bearing an *ortho*-ethynyl substituent, does not react with either *i*-Pr_2NH or ethylenediamine to furnish the ring-closed species **VIII** (Fig. 2d) or a hydroamination product, respectively.

PE3 investigated whether the presence of a borinic acid substituent in the substrate is mandatory for a cyclization reaction. Indeed, the decisive role of the MesBOH group was confirmed since the bis(2-bromophenyl)butadiyne ($\mathbf{B_0}$) remained inert toward ethylenediamine at room temperature—even after addition of 2 eq. $PhB(OH)_2$ (above 60 °C, progressive decomposition was observed).[65] A 1 : 1 mixture of the *ortho*-butadiynyl-

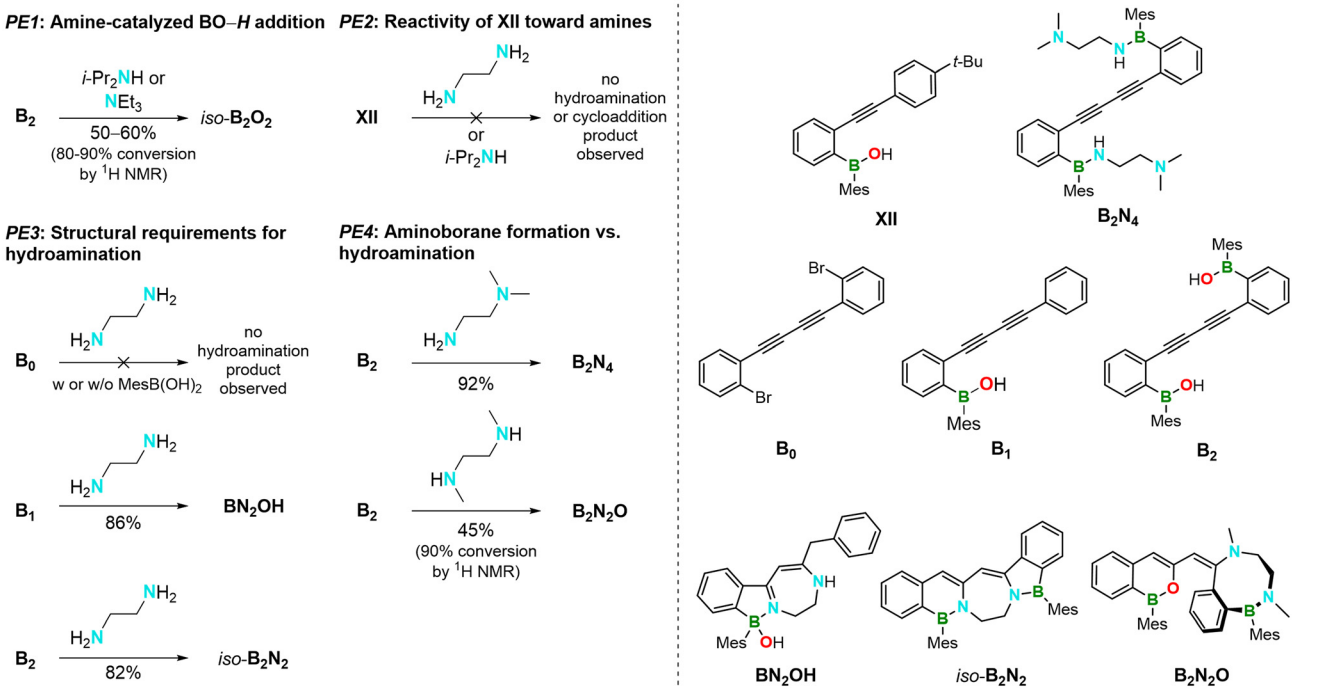

Fig. 5 Probe experiments *PE1*–*PE4* designed to elucidate key mechanistic aspects of the amine-promoted cyclization reactions of the butadiynylene-bridged bisborinic acid $\mathbf{B_2}$, leading to *iso*-$\mathbf{B_2O_2}$ and *iso*-$\mathbf{B_2N_2}$. All reactions were carried out in THF, either at temperatures up to 60 °C (*PE1* and *PE2*) or at room temperature (*PE3* and *PE4*).

substituted monoborinic acid $\mathbf{B_1}$ and ethylenediamine furnished the double-hydroamination product $\mathbf{BN_2OH}$ (86%),[66] which was structurally characterized by SCXRD (Fig. 6).[67] The N-bonded H atom was located in the difference electron-density map. The ^{11}B NMR spectrum of $\mathbf{BN_2OH}$ displays a signal at 7.8 ppm, consistent with the presence of a tetracoordinate B nucleus.[68,69] As noted previously, introduction of two MesBOH substituents ($\mathbf{B_2}$) leads to the formation of the fully cyclized product *iso*-$\mathbf{B_2N_2}$ (82%).

PE4 unveiled how *N*-methylation of ethylenediamine can be used to mask part of its reactive N–H bonds and interrupt the reaction cascade at strategic points. *N*,*N*-Dimethylethylenediamine ($Me_2NCH_2CH_2NH_2$; 2 eq.)[70] reacts with $\mathbf{B_2}$ without adding across the C≡C bonds, giving the ditopic aminoborane $\mathbf{B_2N_4}$ in 92% yield (Fig. 5). SCXRD, analysis of $\mathbf{B_2N_4}$ confirms the presence of two B–NH moieties and a linear butadiyne core (Fig. 6). In solution, NMR spectroscopy revealed an N*H* signal at $\delta(^1H)$ = 6.42 and C≡C resonances at $\delta(^{13}C)$ = 84.0 and 77.1. Reaction of *N*,*N*′-dimethylethylenediamine (Me(H)NCH_2CH_2N(H)Me; 1 eq. or 2 eq.) with $\mathbf{B_2}$ affords the doubly cyclized compound $\mathbf{B_2N_2O}$. According to SCXRD, $\mathbf{B_2N_2O}$, like $\mathbf{BN_2OH}$, features one aminoborane moiety (Fig. 6). Moreover, the boron-free N–H functionality underwent a *cis*-hydroamination reaction with the adjacent C≡C bond, while the distal C≡C bond participated in a corresponding *trans*-O–H-addition reaction, generating a six-membered C_4BO ring. The N-appended C≡C bond in $\mathbf{B_2N_2O}$ adopts the sterically favored *E*-configuration. The eight-membered C_5BN_2-heterocycle, which assumes a boat-like conformation, imparts a distinct three-dimensional structure to $\mathbf{B_2N_2O}$.

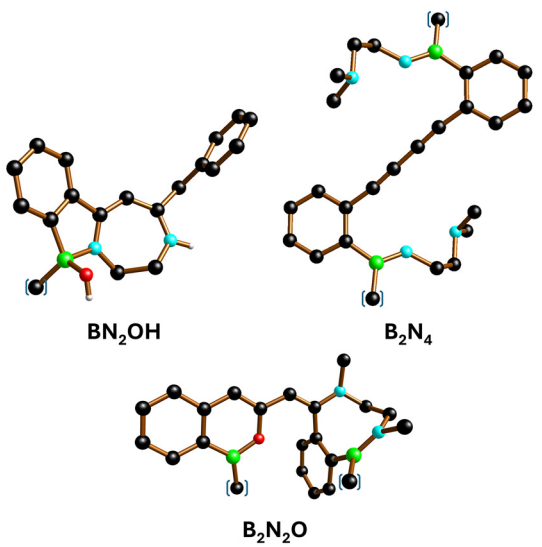

Fig. 6 Solid-state structures of $\mathbf{BN_2OH}$ (left), $\mathbf{B_2N_4}$ (right), and $\mathbf{B_2N_2O}$ (bottom). H: white, B: green, C: black, N: cyan, O: red. For clarity, only the *ipso*-C atoms of the Mes substituents are shown; C–*H* atoms are omitted.

Taken together, probe experiments and the literature precedents lead to the following conclusions:

PE1 suggests that the amine catalysts act mainly as Brønsted bases, likely promoting deprotonation of the BO–H units in the substrate and thereby lowering the barrier for nucleophilic attack at the C≡C bonds.[71] In this context, it is pertinent to ask why *i*-Pr_2NH does not itself undergo hydroamination at the diphenylbutadiyne core but instead mediates the BO–H addition. A straightforward explanation lies in the substantial steric demand of this amine (*cf. LP1*: even in the case of the sterically unencumbered butadiyne, secondary amines add once at most). It is also conceivable that intermolecular *i*-Pr_2NH addition is reversible to such an extent that intramolecular cyclization reactions ultimately prevail (*cf. LP1*: facile exchange of an NR_2 substituent for an N(H)R substituent).[72]

PE2 indicates that the reactive[73,74] butadiyne core is essential as the substrate in the cyclization reactions. Differing from the cases where very strong added bases shift the RE–H-deprotonation equilibrium markedly toward the RE^- nucleophile (E = RN, O), the weaker bases employed in the present study exert a less pronounced activating effect. Consequently, the C≡C bond to be attacked must possess a higher degree of electrophilicity, which is conferred by the adjacent, electron-withdrawing C≡C moiety in the butadiynyl substituent.

PE3 shows that the absence of MesBOH substituents in the diphenylbutadiyne starting material suppresses hydroamination—a remarkable contrast to the behavior of parent butadiyne, C_2H_4 (*cf. LP2*). The lack of $\mathbf{B_0}$ reactivity has probably steric reasons and cannot be remedied by the addition of external $PhB(OH)_2$. It therefore appears plausible that the reaction cascade from $\mathbf{B_2}$ to *iso*-$\mathbf{B_2N_2}$ is initiated by the formation of at least one B–N bond, rendering subsequent hydroamination a kinetically and entropically favored intramolecular process.[75] Indeed, after the introduction of a single MesBOH moiety into the diphenylbutadiyne scaffold, the resulting compound $\mathbf{B_1}$ reacts readily with ethylenediamine to yield $\mathbf{BN_2OH}$, whose N–C-bond pattern matches that in *iso*-$\mathbf{B_2N_2}$.[68] An important overall conclusion from *PE3* is thus that a single MesBOH substituent in the starting material is sufficient to drive the entire 1,3-bisaddition sequence on the diphenylbutadiyne core.

PE4 demonstrates that B–N-bond formation proceeds in high yields in our system. The free NMe_2 substituent in $\mathbf{B_2N_4}$, which could in principle act as a hydroamination catalyst similar to NEt_3, does not induce cyclization at the two remaining N–H bonds. A possible explanation is that a B-bonded N–H functionality is no longer capable of addition across a C≡C bond, as the nucleophilicity of its N atom is now diminished by N═B π-donation. This implies that, in the formation of *iso*-$\mathbf{B_2N_2}$, the remote NH_2 group remaining after aminoborane formation adds to the diphenylbutadiyne unit—an outcome not possible for $\mathbf{B_2N_4}$, where the pendant substituent is NMe_2. The overall addition pattern in $\mathbf{B_2N_2O}$ differs markedly from that in $\mathbf{B_2O_2}$ (which exhibits C–E bonds in vicinal positions), but resembles that in *iso*-$\mathbf{B_2O_2}$ and *iso*-$\mathbf{B_2N_2}$ (C–E bonds separated by a $C(sp^2)$–H unit), reflecting the trend established in *LP1*, *LP2*, and in our previous amine-catalyzed cyclization reactions [*cf. PE3*]. $\mathbf{B_2N_2O}$ is not a naphthylbenzofulvene derivative, ruling out the possibility that the observed 1,3-bisaddition pattern arises from a preference for this structural motif. The presence of the mixed BO/BN heterocyclic scaffold can, in light of *LP1*, be attributed to the fact that $Me(H)NCH_2CH_2N(H)Me$ contains secondary amines at both positions that add only once to butadiyne (and then at the terminal position). This leaves one C≡C bond available for the formation of the C_4BO ring.

Quantum-chemical study of the amine-catalyzed cyclization of B_2 leading to *iso*-B_2O_2

Treatment of $\mathbf{B_2}$ with amines (NEt_3, *i*-Pr_2NH, or ethylenediamine) leads to asymmetric O- or N-addition, forming one five- and one six-membered ring (*cf. iso*-$\mathbf{B_2O_2}$ and *iso*-$\mathbf{B_2N_2}$). For a quantum-chemical assessment of the relevant elementary steps leading to the observed structural motif, we selected the NEt_3-catalyzed cyclization of $\mathbf{B_2}$ as a representative model system, thus bypassing complexities arising from preceding aminoborane formation, as would need to be considered in the case of *iso*-$\mathbf{B_2N_2}$. Various mechanisms were examined, while the most favorable pathway, both thermodynamically and kinetically, is depicted in Fig. 7 and discussed below:

Consistent with the conclusions drawn from *PE1*, the BO–*H* moiety of $\mathbf{B_2}^c$ initially forms a hydrogen bond with NEt_3 in a barrierless, weakly exergonic process furnishing **INT-1**. The subsequent transition state TS_{1-2} for the 5-*exo-dig* cyclization is accessible at room temperature ($\Delta G^{\ddagger}$ = 17.3 kcal mol^{-1}) and involves simultaneous abstraction of the BO–*H* proton, formation of an O–C-bond, and generation of a (formally) deprotonated 1,3-enyne unit.[76] The resulting $[HNEt_3]^+$ cation remains associated with the endocyclic O atom through an N–H···O hydrogen bond in the ensuing five-membered-ring intermediate **INT-2** (ΔG = 9.1 kcal mol^{-1}). In comparison, the barrier for the conceivable alternative formation of a six-membered-ring compound is significantly higher (25.2 kcal mol^{-1} *vs.* 17.3 kcal mol^{-1}), consistent with *LP1*, which reports that parent butadiyne reacts with primary or secondary amines preferentially in 1-position (*cf.* **IX** in Fig. 4).[77] In a subsequent slightly exergonic isomerization step, the enyne anion **INT-2** is converted into a cumulene anion, which acquires a proton from the nearby second borinic acid substituent to afford **INT-3** *via* the energetically low-lying transition state TS_{2-3}.[78] A facile approximate 180° flip of the borylated phenyl ring brings its $[B–O]^-$ group into proximity with $[HNEt_3]^+$, enabling H^+ transfer and the pronouncedly exergonic formation of cumulene **INT-4** (ΔG = −12.8 kcal mol^{-1}). Stabilization of the enyne anion generated in the first cyclization step *via* cumulene formation, which concomitantly places the carbanionic center near the proton source BO–H, is possible only for butadiyne substrates but not for simple alkynes, thereby rationalizing the experimental findings of *PE2*. The second cyclization step *via* TS_{4-5} has the highest activation barrier of $\Delta G^{\ddagger}$ = 24.4 kcal mol^{-1}, which explains why the reaction had to be performed at 60 °C to obtain *iso*-$\mathbf{B_2O_2}$ in reasonable yields within a practical timespan. From **INT-4**, nucleophilic attack of the O nucleophile at the cumulene affords the deprotonated buta-

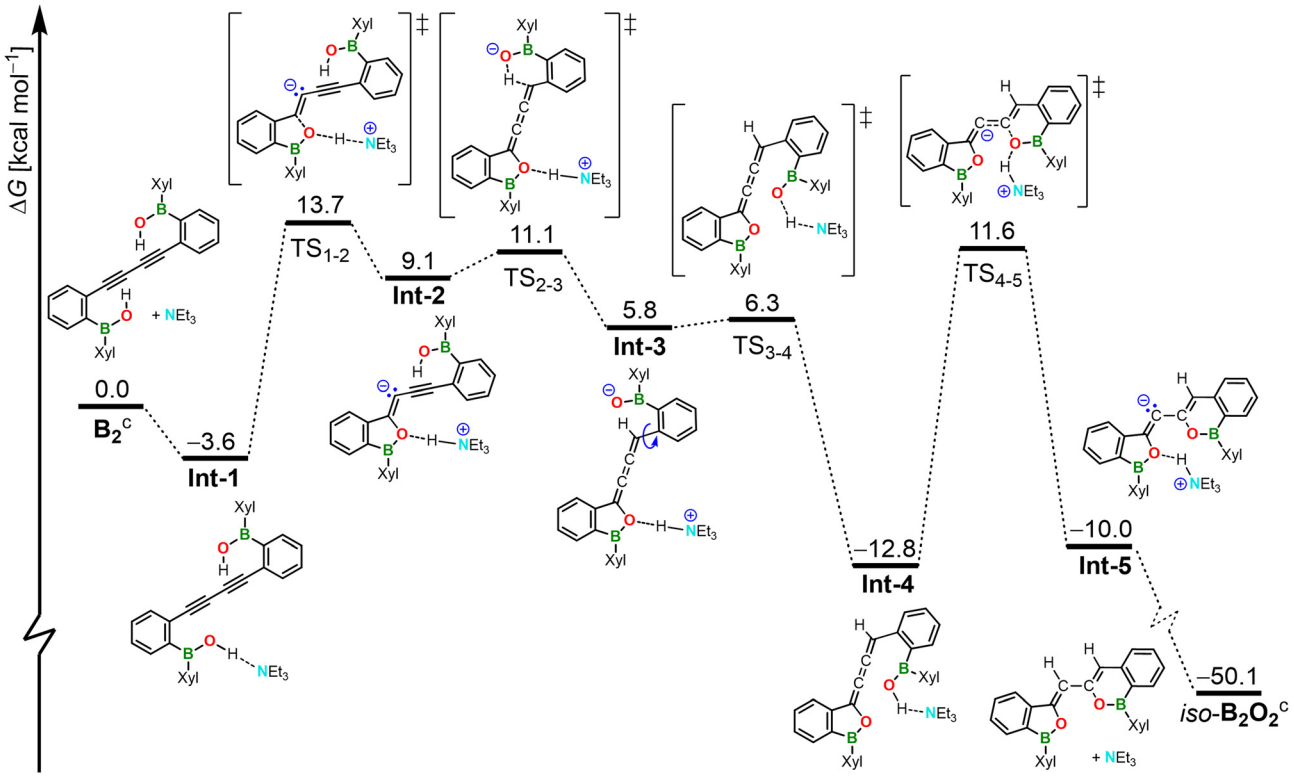

Fig. 7 Computed reaction mechanism for the NEt_3-catalyzed double cyclization of $\mathbf{B_2}$ furnishing *iso*-$\mathbf{B_2O_2}$. Gibbs free energy changes (ΔG) were calculated at the ωB97X-D/6-311+G(d,p), CPCM(THF) level of theory.[39,40] *Note*: To facilitate convergence of intermediates and transition states, *ortho*-xylyl (Xyl) instead of mesityl (Mes) substituents were used; to distinguish the computed Xyl-bearing starting material and product from the real Mes-bearing ones, the former were denoted as $\mathbf{B_2}^c$ and *iso*-$\mathbf{B_2O_2}^c$.

diene **INT-5** in a mildly endergonic step.[79] Subsequently, the $[HNEt_3]^+$ cation migrates beneath the anion plane from the O atom toward the carbanion, followed by N-to-C proton transfer. This process provides a strong thermodynamic driving force for the formation of *iso*-$\mathbf{B_2O_2}^c$ (ΔG = −50.1 kcal mol^{-1}; details of this final step, as well as the thermodynamics and kinetics of *syn*/*anti*-interconversion, are provided in Fig. S134).

Conclusions

Single- and double-Au(I)-catalyzed cyclizations of *ortho*-butadiynyl-substituted arylborinic acids provide efficient access to BO-doped polycyclic aromatic hydrocarbons bearing fluorescence-enhancing alkynyl substituents (*cf.* **BO**) and to $(BO)_2$-doped biaryls, respectively (*cf.* $\mathbf{B_2O_2}$). Remarkably, this approach can be extended beyond the precious-metal ion, as simple amines such as NEt_3 are also capable of catalyzing the reaction, while steering it toward a distinct connectivity pattern: whereas the 2,3-OC-addition realized in $\mathbf{B_2O_2}$ is characteristic of the Au(I)-catalyzed double cyclization of *o*,*o*′-bis[MesB(OH)]-diphenylbutadiyne ($\mathbf{B_2}$), the NEt_3-promoted pathway leads to 1,3-OC-addition, furnishing the isomeric $(BO)_2$-naphthylbenzofulvene *iso*-$\mathbf{B_2O_2}$. Even more strikingly, treatment of $\mathbf{B_2}$ with ethylenediamine generates the corresponding $(BN)_2$-doped framework *iso*-$\mathbf{B_2N_2}$ in the absence of any additional catalyst. A plausible mechanistic scenario for the formation of *iso*-$\mathbf{B_2O_2}$ was established through a combination of probe experiments and quantum-chemical calculations: in a concerted process, the Brønsted base NEt_3 engages the proton of the first borinic acid group, thereby enhancing the nucleophilicity of the appended O atom, which simultaneously adds to the adjacent C≡C bond. We demonstrated that (i) the C≡C bond becomes sufficiently electrophilic for this attack due to the electron-withdrawing effect of the attached ethynyl moiety, and (ii) the BO-benzofulvene unit preferentially forms instead of a BO-naphthyl group due to more favorable kinetics. This step is followed by the formation of a cumulene intermediate, which subsequently reacts with the second borinic acid group, this time forming the BO-naphthyl unit of *iso*-$\mathbf{B_2O_2}$. The mechanistic understanding gained in this study builds a foundation for the development of novel and versatile synthetic tools to access $(BE)_n$-doped PAHs with desirable optoelectronic properties.

Author contributions

S. M. M. performed the experimental studies and characterized all new compounds. J. K. performed the quantum chemical

calculations. A. V. V. and E. P. performed the X-ray crystal structure analyses of all compounds. H.-W. L., H. H., and M. W. supervised the project. The manuscript was written by S. M. M. and M. W. and edited by all co-authors.

Conflicts of interest

There are no conflicts to declare.

Data availability

The supporting data has been provided as part of the supplementary information (SI). Supplementary information: synthetic procedures, NMR spectra, photophysical and electrochemical data, X-ray crystallographic data and computational details. See DOI: https://doi.org/10.1039/d6dt00412a.

CCDC 2523153–2523170 contain the supplementary crystallographic data for this paper.[80a–r]

Acknowledgements

The authors are grateful to the Deutsche Forschungsgemeinschaft (DFG) for financial support (GZ: SFB 1762/1 2026; project number: 551403841). S. M. M. wishes to thank the Fonds der Chemischen Industrie (FCI) for a Kekulé Ph.D. grant. Parts of this research were carried out on the P24 beamline (projects I-20231039, R-20240674, and R-20250872) at PETRA III at DESY, a member of the Helmholtz Association (HGF). We thank Dr M. Tolkiehn and Dr P. Pokhriyal for their assistance regarding the use of the beamline P24. We gratefully thank Prof B. Engels for fruitful discussions, G. Sentis for assistance with NMR measurements, and PD M. Braun for discussion of the UV/Vis spectra. We acknowledge O. Ouadoudi ($\mathbf{B_2}$) and J. M. Rüger ($\mathbf{B_1}^{SI}$) for their assistance with the synthesis of starting materials.

References

1 A. Borissov, Y. K. Maurya, L. Moshniaha, W.-S. Wong, M. Żyła-Karwowska and M. Stępień, *Chem. Rev.*, 2022, **122**, 565–788, DOI: 10.1021/acs.chemrev.1c00449.
2 M. Hirai, N. Tanaka, M. Sakai and S. Yamaguchi, *Chem. Rev.*, 2019, **119**, 8291–8331, DOI: 10.1021/acs.chemrev.8b00637.
3 M. Stępień, E. Gońka, M. Żyła and N. Sprutta, *Chem. Rev.*, 2017, **117**, 3479–3716, DOI: 10.1021/acs.chemrev.6b00076.
4 Z. X. Giustra and S.-Y. Liu, *J. Am. Chem. Soc.*, 2018, **140**, 1184–1194, DOI: 10.1021/jacs.7b09446.
5 G. Bélanger-Chabot, H. Braunschweig and D. K. Roy, *Eur. J. Inorg. Chem.*, 2017, **2017**, 4353–4368, DOI: 10.1002/ejic.201700562.
6 H. Helten, *Chem. – Eur. J.*, 2016, **22**, 12972–12982, DOI: 10.1002/chem.201602665.
7 P. G. Campbell, A. J. V. Marwitz and S.-Y. Liu, *Angew. Chem., Int. Ed.*, 2012, **51**, 6074–6092, DOI: 10.1002/anie.201200063.
8 Z. Liu and T. B. Marder, *Angew. Chem., Int. Ed.*, 2008, **47**, 242–244, DOI: 10.1002/anie.200703535.
9 J. S. A. Ishibashi, A. Dargelos, C. Darrigan, A. Chrostowska and S.-Y. Liu, *Organometallics*, 2017, **36**, 2494–2497, DOI: 10.1021/acs.organomet.7b00296.
10 M. Franceschini, M. Crosta, R. R. Ferreira, D. Poletto, N. Demitri, J. P. Zobel, L. González and D. Bonifazi, *J. Am. Chem. Soc.*, 2022, **144**, 21470–21484, DOI: 10.1021/jacs.2c06803.
11 S. Jeong, E. Park, J. Kim, S. B. Park, S. H. Kim, W. Choe, J. Kim and Y. S. Park, *Angew. Chem., Int. Ed.*, 2023, **62**, e202314148, DOI: 10.1002/anie.202314148.
12 V. C. Wakchaure, M. M. Lorenzo-García, F. Fasano, M. Crosta, N. Biot, N. Demitri, P. K. Mondal, B. D. Ward and D. Bonifazi, *Angew. Chem., Int. Ed.*, 2025, **64**, e202416700, DOI: 10.1002/anie.202416700.
13 H. Lee, M. Fischer, B. K. Shoichet and S.-Y. Liu, *J. Am. Chem. Soc.*, 2016, **138**, 12021–12024, DOI: 10.1021/jacs.6b06566.
14 K. Boknevitz, J. S. Italia, B. Li, A. Chatterjee and S.-Y. Liu, *Chem. Sci.*, 2019, **10**, 4994–4998, DOI: 10.1039/c8sc05167d.
15 T. Kaehler, M. Bolte, H.-W. Lerner and M. Wagner, *Angew. Chem., Int. Ed.*, 2019, **58**, 11379–11384, DOI: 10.1002/anie.201905823.
16 O. Ouadoudi, T. Kaehler, M. Bolte, H.-W. Lerner and M. Wagner, *Chem. Sci.*, 2021, **12**, 5898–5909, DOI: 10.1039/d1sc00543j.
17 E. Januszewski, M. Bolte, H.-W. Lerner and M. Wagner, *Organometallics*, 2012, **31**, 8420–8425, DOI: 10.1021/om300990z.
18 A. Abengózar, D. Sucunza, P. García-García and J. J. Vaquero, *Beilstein J. Org. Chem.*, 2019, **15**, 1257–1261, DOI: 10.3762/bjoc.15.122.
19 O. Ouadoudi, T. Kaehler, E. G. Çevik, M. Bolte, B. Stöger, A. Virovets, H.-W. Lerner and M. Wagner, *Dalton Trans.*, 2022, **51**, 13195–13198, DOI: 10.1039/d2dt02364d.
20 I. Baraldi, M. C. Bruni, M. Caselli and G. Ponterini, *J. Chem. Soc., Faraday Trans. 2*, 1989, **85**, 65–74, DOI: 10.1039/F29898500065.
21 S. Scheiner, S. J. Grabowski and T. Kar, *J. Phys. Chem. A*, 2001, **105**, 10607–10612, DOI: 10.1021/jp0131267.
22 G. R. Desiraju, *Chem. Commun.*, 2005, 2995–3001, DOI: 10.1039/b504372g.
23 C. Jelsch and Y. B. M. Bisseyou, *IUCrJ*, 2017, **4**, 158–174, DOI: 10.1107/S2052252516020200.
24 K. Dodou, *Expert Opin. Invest. Drugs*, 2005, **14**, 1419–1434, DOI: 10.1517/13543784.14.11.1419.
25 C. L. Beisel, M. K. Dowd and P. J. Reilly, *J. Mol. Struct.: THEOCHEM*, 2005, **730**, 51–58, DOI: 10.1016/j.theochem.2005.05.010.
26 S. Chatterjee, N. M. Tripathi and A. Bandyopadhyay, *Chem. Commun.*, 2021, **57**, 13629–13640, DOI: 10.1039/d1cc05481c.

27 R. J. Grams, W. L. Santos, I. R. Scorei, A. Abad-García, C. A. Rosenblum, A. Bita, H. Cerecetto, C. Viñas and M. A. Soriano-Ursúa, *Chem. Rev.*, 2024, **124**, 2441–2511, DOI: 10.1021/acs.chemrev.3c00663.
28 G. F. S. Fernandes, W. A. Denny and J. L. Dos Santos, *Eur. J. Med. Chem.*, 2019, **179**, 791–804, DOI: 10.1016/j.ejmech.2019.06.092.
29 A. John, S. Kirschner, M. K. Fengel, M. Bolte, H.-W. Lerner and M. Wagner, *Dalton Trans.*, 2019, **48**, 1871–1877, DOI: 10.1039/c8dt04820g.
30 I. M. Hunsberger, R. Ketcham and H. S. Gutowsky, *J. Am. Chem. Soc.*, 1952, **74**, 4839–4845, DOI: 10.1021/ja01139a032.
31 Emission wavelengths refer to the highest-intensity maxima of the vibrationally resolved bands.
32 For convenience, we will henceforth use the term "hydroamination", although the reacting species is, strictly speaking, not an amine but an aminoborane.
33 C. Hoffend, M. Diefenbach, E. Januszewski, M. Bolte, H.-W. Lerner, M. C. Holthausen and M. Wagner, *Dalton Trans.*, 2013, **42**, 13826–13837, DOI: 10.1039/c3dt51035b.
34 D. H. O'Brien, A. J. Hart and C. R. Russel, *J. Am. Chem. Soc.*, 1975, **97**, 4410–4412, DOI: 10.1021/ja00848a054.
35 N. S. Mills, E. E. Burns, J. Hodges, J. Gibbs, E. Esparza, J. L. Malandra and J. Koch, *J. Org. Chem.*, 1998, **63**, 3017–3022, DOI: 10.1021/jo972202s.
36 R. Shenhar, R. Beust, R. E. Hoffman, I. Willner, H. E. Bronstein, L. T. Scott and M. Rabinovitz, *J. Org. Chem.*, 2001, **66**, 6004–6013, DOI: 10.1021/jo010103f.
37 The number in square brackets refers to the standard deviation after averaging all geometric parameters of the same type.
38 S. Kiviniemi, M. Nissinen, T. Alaviuhkola, K. Rissanen and J. Pursiainen, *J. Chem. Soc., Perkin Trans. 2*, 2001, 2364–2369, DOI: 10.1039/b100775k.
39 J.-D. Chai and M. Head-Gordon, *Phys. Chem. Chem. Phys.*, 2008, **10**, 6615–6620, DOI: 10.1039/b810189b.
40 (*a*) R. Krishnan, J. S. Binkley, R. Seeger and J. A. Pople, *J. Chem. Phys.*, 1980, **72**, 650–654, DOI: 10.1063/1.438955; (*b*) T. Clark, J. Chandrasekhar, G. W. Spitznagel and P. von Ragué Schleyer, *J. Comput. Chem.*, 1983, **4**, 294–301, DOI: 10.1002/jcc.540040303; (*c*) V. Barone and M. Cossi, *J. Phys. Chem. A*, 1998, **102**, 1995–2001, DOI: 10.1021/jp9716997.
41 Y. Shibuya, K. Aonuma, T. Kimura, T. Kaneko, W. Fujiwara, Y. Yamaguchi, D. Kumaki, S. Tokito and H. Katagiri, *J. Phys. Chem. C*, 2020, **124**, 4738–4746, DOI: 10.1021/acs.jpcc.9b11214.
42 N. K. Lee, S. Park, M.-H. Yoon, Z. H. Kim and S. K. Kim, *Phys. Chem. Chem. Phys.*, 2012, **14**, 840–848, DOI: 10.1039/c1cp22854d.
43 F. Zhang, G. B. Bacskay and S. H. Kable, *J. Phys. Chem. A*, 2004, **108**, 172–184, DOI: 10.1021/jp036271o.
44 J. L. Del Riccio, F. Zhang, A. R. Lacey and S. H. Kable, *J. Phys. Chem. A*, 2000, **104**, 7442–7451, DOI: 10.1021/jp000166m.
45 M. Fadouach, B. Benali, A. Kadiri, C. Cazeau-Dubroca and G. Nouchi, *Spectrochim. Acta*, 1992, **48**, 1491–1500, DOI: 10.1016/0584-8539(92)80156-Q.
46 For 2,2′-binaphthyl, the values of λ_{abs}^{ons} and λ_{em}^{max} had to be estimated from the corresponding spectral plots provided in the cited publications and are therefore subject to uncertainties of about ±5 nm.
47 Compared to the $(BO)_2$-binaphthyl $\mathbf{B_2O_2}$, the π-extended $(BO)_2$-bianthryl $\mathbf{B_2O_2}^{SI}$ absorbs and emits further toward the red with λ_{abs}^{ons}= 395 nm, λ_{em}^{max}= 437 nm, and Φ_{PL} = 50%.
48 R. Dorel and A. M. Echavarren, *Chem. Rev.*, 2015, **115**, 9028–9072, DOI: 10.1021/cr500691k.
49 C. M. Krauter, A. S. K. Hashmi and M. Pernpointner, *ChemCatChem*, 2010, **2**, 1226–1230, DOI: 10.1002/cctc.201000136.
50 L. Benhamou, D. W. Walker, B.-K. Bučar, A. E. Aliev and T. D. Sheppard, *Org. Biomol. Chem.*, 2016, **14**, 8039–8043, DOI: 10.1039/c6ob01419d.
51 J. Escorihuela, A. Lledós and G. Ujaque, *Chem. Rev.*, 2023, **123**, 9139–9203, DOI: 10.1021/acs.chemrev.2c00482.
52 Z. Tashrifi, M. M. Khanaposhtani, M. Biglar, B. Larijani and M. Mahdavi, *Asian J. Org. Chem.*, 2020, **9**, 969–991, DOI: 10.1002/ajoc.202000092.
53 T. E. Müller, K. C. Hultzsch, M. Yus, F. Foubelo and M. Tada, *Chem. Rev.*, 2008, **108**, 3795–3892, DOI: 10.1021/cr0306788.
54 R. Severin and S. Doye, *Chem. Soc. Rev.*, 2007, **36**, 1407–1420, DOI: 10.1039/b600981f.
55 S. Gupta, P. K. Agarwal, M. Saifuddin and B. Kundu, *Tetrahedron Lett.*, 2011, **52**, 5752–5757, DOI: 10.1016/j.tetlet.2011.08.079.
56 M. Patel, R. K. Saunthwal and A. K. Verma, *Acc. Chem. Res.*, 2017, **50**, 240–254, DOI: 10.1021/acs.accounts.6b00449.
57 D. Tzalis, C. Koradin and P. Knochel, *Tetrahedron Lett.*, 1999, **40**, 6193–6195, DOI: 10.1016/S0040-4039(99)01133-8.
58 T. Imahori, C. Hori and Y. Kondo, *Adv. Synth. Catal.*, 2004, **346**, 1090–1092, DOI: 10.1002/adsc.200404076.
59 W. Schroth, J. Peschel and A. Zschunke, *Z. Chem.*, 1969, **9**, 108–109, DOI: 10.1002/zfch.19690090309.
60 W. Schroth, J. Peschel and A. Zschunke, *Z. Chem.*, 1969, **9**, 110–111, DOI: 10.1002/zfch.19690090310.
61 This applies to alkylamines; primary aromatic amines undergo addition at the 3-position without substitution of the NR_2 group: ref. 59.
62 W. Schroth, J. Peschel and A. Zschunke, *Z. Chem.*, 1969, **9**, 143, DOI: 10.1002/zfch.19690090408.
63 W. Schroth, A. Preiß, M. Bethin and W.-D. Bartsch, *Z. Chem.*, 1977, **17**, 216–218, DOI: 10.1002/zfch.19770170605.
64 W. W. Paudler and A. G. Zeiler, *J. Org. Chem.*, 1969, **34**, 999–1001, DOI: 10.1021/jo01256a050.
65 The dibrominated derivative was employed to mimic, at least in part, the steric bulk imposed by the boryl substituents in $\mathbf{B_2}$.
66 ^{1}H- and ^{13}C{^{1}H} NMR spectra were recorded at room temperature in $CDCl_3$. The saturated CH_2 moiety bearing the phenyl

ring gives rise to resonances at $\delta(^1H)$ = 3.77 (s, 2H) and $\delta(^{13}C)$ = 43.8. The ^1H NMR spectrum further displays a signal at 5.63 ppm (1H) that shows no cross-peak in the HSQC experiment and has a pronouncedly temperature-dependent chemical shift value: at 50 °C, the resonance shifts upfield to 5.50 ppm. This signal may well correspond to an N–*H* proton, although assignment to the BO–*H* proton cannot be excluded (with the respective other proton resonance remaining undetected). The central CH group of the seven-membered ring gives rise to signals at $\delta(^1H)$ = 5.65 (1H) and $\delta(^{13}C)$ = 86.8; the two N*C*(sp^2) atoms are detected at $\delta(^{13}C)$ = 166.5 and 161.1. For comparison, the resonances of the central CH_2 groups in various 3*H*-1,5-benzodiazepines (which correspond to the 2,3-dihydro-6*H*-1,4-diazepine tautomer of **BN_2OH**) appear at significantly higher field (around $\delta(^1H) \approx 2.8$; motionally broadened signal) and $\delta(^{13}C) \approx 35$. Consistent with our observations, ^{13}C chemical shift values of N*C*(sp^2) moieties in verified 2,3-dihydro-1*H*-1,4-diazepine tautomers have been reported in the range 155.6–170.8 ppm. Taken together, the available evidence supports assignment of **BN_2OH** to the 2,3-dihydro-1*H*-1,4-diazepine tautomer rather than to the diimine tautomer 2,3-dihydro-6*H*-1,4-diazepine: (*a*) Z.-Y. Ding, F. Chen, J. Qin, Y.-M. He and Q.-H. Fan, *Angew. Chem., Int. Ed.*, 2012, **51**, 5706–5710, DOI: 10.1002/anie.201200309; (*b*) J. C. L. Menezes, L. B. A. Vaz, P. Melo De Abreu Vieira, K. Da Silva Fonseca, C. M. Carneiro and J. G. Taylor, *Molecules*, 2014, **20**, 43–51, DOI: 10.3390/molecules20010043; (*c*) A. R. Romanov, A. Y. Rulev, I. A. Ushakov, V. M. Muzalevskiy and V. G. Nenajdenko, *Mendeleev Commun.*, 2014, **24**, 269–271, DOI: 10.1016/j.mencom.2014.09.007.

67 Bond-length alternation within the unsaturated portion of the seven-membered heterocycle is less pronounced than suggested by the structural formula in Fig. 5, with distances of 1.316(2) [N=C], 1.332(2) [N(H)–C], 1.415(2) [C–C], and 1.388(2) Å [C=C], indicating a considerable π-delocalization. These values can be compared with those of the (largely) localized single and double bonds in an (adamantyl)(methyl)vinyl amine derivative with a torsion angle of almost 90° about the *N*-vinyl bond (1.414(3) Å; CSD: BEYCEO), in $[H_2C(C(Me)=N(Me))_2BF_2][PF_6]$ (1.269(5)/1.274(5) Å; CSD: JENLUJ), $H_2CC(H)–C(H)CH_2$ (1.47 Å), and $H_2C=CH_2$ (1.34 Å); fully delocalized C–N bonds are found in $HC(C(Me)N(Me))_2BF_2$ (1.324(2) Å; CSD: JENLOD): (*a*) N. Kuhn, A. Kuhn, M. Speis, D. Bläser and R. Boese, *Chem. Ber.*, 1990, **123**, 1301–1306, DOI: 10.1002/cber.19901230613; (*b*) S. Solé, X. Cattoën, H. Gornitzka, D. Bourissou and G. Bertrand, *Tetrahedron Lett.*, 2004, **45**, 5391–5393, DOI: 10.1016/j.tetlet.2004.05.082; (*c*) M. A. Fox and J. K. Whitesell, *Organic Chemistry*, Jones and Bartlett Publishers, Inc., Boston, Toronto, London, Singapore, 3rd edn, 2004.

68 It remains to be conclusively determined which subtle factors lead to the addition of an H_2O molecule in the case of **BN_2OH**, whereas no such addition occurs to *iso*-**B_2N_2**. The cause is likely not related to the B center, which should be electronically well-saturated in **BN_2OH** due to tetracoordination and in *iso*-**B_2N_2** due to N=B π-donation. Instead, H_2O addition may be driven by the R–CH_2–Ph fragment in **BN_2OH**. This fragment is rotatable about the R–CH_2 bond and can thus avoid unfavorable steric interactions by adopting an orthogonal orientation of the phenyl group relative to the C_5N_2-heterocycle (*cf.* the solid-state conformation of **BN_2OH** in Fig. 6). In the H_2O-elimination product of **BN_2OH**, such rotation is prevented by the pronounced double-bond character of the R=CH–Ph fragment, and the Ph-ring (in both the planarized *E*- and *Z*-configurations) would experience steric strain. In the case of *iso*-**B_2N_2**, such steric strain is not an issue, because the two potentially colliding H-atoms in the *Z*-configuration (fjord region) are replaced by the bridging B atom.

69 H. Nöth and B. Wrackmeyer, *Nuclear Magnetic Resonance Spectroscopy of Boron Compounds*, Springer Berlin Heidelberg, Berlin, Heidelberg, 1978.

70 The corresponding reaction with 1 eq. $Me_2NCH_2CH_2NH_2$ lacks selectivity. We confirmed that **B_2** was not fully consumed; no signatures of vinylic moieties were detected.

71 For reasons that are not yet fully understood, *N*,*N*′,*N*′,*N*′-tetramethylethylenediamine does not act as a cyclization catalyst for **B_2**. Addition of elemental Hg to the reaction mixture did not affect the reaction progress, further supporting the assumption that the process is genuinely organocatalytic and not facilitated by adventitious transition-metal clusters and complexes (note, however, that the 'mercury drop test' has known limitations and, *e.g.*, failed to suppress the Au(I)-catalyzed formation of **B_2O_2**): V. M. Chernyshev, A. V. Astakhov, I. E. Chikunov, R. V. Tyurin, D. B. Eremin, G. S. Ranny, V. N. Khrustalev and V. P. Ananikov, *ACS Catal.*, 2019, **9**, 2984–2995, DOI: 10.1021/acscatal.8b03683.

72 In this sense, the addition of H_2O, released during reactions proceeding *via* aminoborane formation (*e.g.*, *iso*-**B_2N_2** synthesis), can also be understood not to compete with the desired ring-closing reactions.

73 T. J. Taylor and F. P. Gabbaï, *Organometallics*, 2006, **25**, 2143–2147, DOI: 10.1021/om060186w.

74 M. R. Bryce, *J. Mater. Chem. C*, 2021, **9**, 10524–10546, DOI: 10.1039/d1tc01406d.

75 This conclusion is also consistent with the fact that the reaction of **B_2** with propylene diamine, presumably due to the longer tether, produces *iso*-**B_2N_2**^{SI} in only 19% yield.

76 In 2-position deprotonated 1,3-enynes have been reported. Selected examples: (*a*) H. Kleijn, M. Tigchelaar, R. J. Bulee, C. J. Elsevier, J. Meijer and P. Vermeer, *J. Organomet. Chem.*, 1982, **240**, 329–333, DOI: 10.1016/S0022-328X(00)86799-6; (*b*) L. Brandsma, H. Hommes, H. D. Verkruijsse, A. J. Kos, W. Neugebauer, W. Baumgärtner and P. von Ragué Schleyer, *Recl. Trav. Chim. Pays-Bas*, 1988, **107**, 286–295, DOI: 10.1002/recl.19881070334; (*c*) M. Schäfer, N. Mahr, J. Wolf and H. Werner, *Angew. Chem., Int. Ed. Engl.*, 1993, **32**, 1315–1318, DOI: 10.1002/anie.199313151.

77 We also examined the base-catalyzed 5-*exo-dig vs.* 6-*endo-dig* cyclizations of an *ortho*-alkynyl-substituted borinic acid model. In general, formation of the six-membered BOC_4

ring is thermodynamically favored, whereas the five-membered BOC_3 ring is the kinetic product. Further details are provided in the SI.

78 Deprotonated allenes as representatives of deprotonated cumulenes have been reported. Selected examples: (*a*) G. Linstrumelle and D. Michelot, *J. Chem. Soc., Chem. Commun.*, 1975, 561–562, DOI: 10.1039/C39750000561; (*b*) D. Michelot, J.-C. Clinet and G. Linstrumelle, *Synth. Commun.*, 1982, **12**, 739–747, DOI: 10.1080/00397918208061912; (*c*) T. Jeffery-Luong and G. Linstrumelle, *Synthesis*, 1982, 738–740, DOI: 10.1055/s-1982-29923; (*d*) J. Mateos-Gil, A. Mondal, M. Castiñeira Reis and B. L. Feringa, *Angew. Chem., Int. Ed.*, 2020, **59**, 7823–7829, DOI: 10.1002/anie.201913132.

79 Deprotonated 1,3-butadienes have been reported. Selected examples: (*a*) S. P. de Visser, L. J. de Koning, W. J. van der Hart and N. M. M. Nibbering, *Recl. Trav. Chim. Pays-Bas*, 1995, **114**, 267–272, DOI: 10.1002/recl.19951140603; (*b*) S. P. de Visser, E. van der Horst, L. J. de Koning, W. J. van der Hart and N. M. M. Nibbering, *J. Mass Spectrom.*, 1999, **34**, 303–310, DOI: 10.1002/(SICI)1096-9888(199904)34:4<303::AID-JMS753>3.0.CO;2-C.

80 (*a*) CCDC 2523153: Experimental Crystal Structure Determination, 2026, DOI: 10.5517/ccdc.csd.cc2qpk11; (*b*) CCDC 2523154: Experimental Crystal Structure Determination, 2026, DOI: 10.5517/ccdc.csd.cc2qpk22; (*c*) CCDC 2523155: Experimental Crystal Structure Determination, 2026, DOI: 10.5517/ccdc.csd.cc2qpk33; (*d*) CCDC 2523156: Experimental Crystal Structure Determination, 2026, DOI: 10.5517/ccdc.csd.cc2qpk44; (*e*) CCDC 2523157: Experimental Crystal Structure Determination, 2026, DOI: 10.5517/ccdc.csd.cc2qpk55; (*f*) CCDC 2523158: Experimental Crystal Structure Determination, 2026, DOI: 10.5517/ccdc.csd.cc2qpk66; (*g*) CCDC 2523159: Experimental Crystal Structure Determination, 2026, DOI: 10.5517/ccdc.csd.cc2qpk77; (*h*) CCDC 2523160: Experimental Crystal Structure Determination, 2026, DOI: 10.5517/ccdc.csd.cc2qpk88; (*i*) CCDC 2523161: Experimental Crystal Structure Determination, 2026, DOI: 10.5517/ccdc.csd.cc2qpk99; (*j*) CCDC 2523162: Experimental Crystal Structure Determination, 2026, DOI: 10.5517/ccdc.csd.cc2qpkbb; (*k*) CCDC 2523163: Experimental Crystal Structure Determination, 2026, DOI: 10.5517/ccdc.csd.cc2qpkcc; (*l*) CCDC 2523164: Experimental Crystal Structure Determination, 2026, DOI: 10.5517/ccdc.csd.cc2qpkdd; (*m*) CCDC 2523165: Experimental Crystal Structure Determination, 2026, DOI: 10.5517/ccdc.csd.cc2qpkff; (*n*) CCDC 2523166: Experimental Crystal Structure Determination, 2026, DOI: 10.5517/ccdc.csd.cc2qpkgg; (*o*) CCDC 2523167: Experimental Crystal Structure Determination, 2026, DOI: 10.5517/ccdc.csd.cc2qpkhh; (*p*) CCDC 2523168: Experimental Crystal Structure Determination, 2026, DOI: 10.5517/ccdc.csd.cc2qpkjj; (*q*) CCDC 2523169: Experimental Crystal Structure Determination, 2026, DOI: 10.5517/ccdc.csd.cc2qpkkk; (*r*) CCDC 2523170: Experimental Crystal Structure Determination, 2026, DOI: 10.5517/ccdc.csd.cc2qpkll.